

Novel post-translational modification learning signature reveals B4GALT2 as an immune exclusion regulator in lung adenocarcinoma

Pengpeng Zhang  ^{1,2}, Dingli Wang,¹ Guangyao Zhou,¹ Shuai Jiang,¹ Ge Zhang,³ Lianmin Zhang,¹ Zhenfa Zhang¹

To cite: Zhang P, Wang D, Zhou G, et al. Novel post-translational modification learning signature reveals B4GALT2 as an immune exclusion regulator in lung adenocarcinoma. *Journal for ImmunoTherapy of Cancer* 2025;13:e010787. doi:10.1136/jitc-2024-010787

► Additional supplemental material is published online only. To view, please visit the journal online (<https://doi.org/10.1136/jitc-2024-010787>).

PZ, DW and GZ contributed equally.

Accepted 23 December 2024



© Author(s) (or their employer(s)) 2025. Re-use permitted under CC BY-NC. No commercial re-use. See rights and permissions. Published by BMJ Group.

For numbered affiliations see end of article.

Correspondence to

Dr Zhenfa Zhang;
zhangzhenfa@tmu.edu.cn

Dr Lianmin Zhang;
zhanglianmin1031@163.com

ABSTRACT

Background Lung adenocarcinoma (LUAD) presents significant challenges in prognosis and treatment efficacy evaluation. While post-translational modifications are known to influence tumor progression, their prognostic value in LUAD remains largely unexplored.

Methods We developed a post-translational modification learning signature (PTMLS) using machine learning techniques, analyzing data from 1231 LUAD patients across seven global cohorts. The signature's efficacy in predicting immunotherapy response was evaluated using 12 immunotherapy cohorts spanning multiple cancer types (n=1201). An in-house LUAD tissue cohort (n=171) was used to validate beta-1,4-galactosyltransferase 2's (B4GALT2's) prognostic significance. The role of B4GALT2 in immune exclusion was investigated through in vivo and in vitro experiments.

Results The established PTMLS exhibited exceptional predictive capabilities in LUAD patient outcomes, surpassing the efficacy of 98 existing LUAD prognostic indicators. The system's predictive value was validated across diverse malignancy categories for immunotherapeutic response assessment. From a biological perspective, significant correlations were observed between PTMLS and immunological parameters, whereby elevated PTMLS levels were characterized by attenuated immune responses and immunologically cold neoplastic features. Within the PTMLS framework, B4GALT2 was identified as a crucial molecular component ($r=0.82$, $p<0.05$), and its heightened expression was linked to unfavorable clinical outcomes in LUAD cases, particularly in specimens exhibiting CD8-depleted phenotypes. The spatial distribution patterns between B4GALT2 and immune cell populations, specifically CD8+ T lymphocytes and CD20+ B lymphocytes, were elucidated through multiplexed immunofluorescence analysis. Laboratory investigations subsequently established B4GALT2's regulatory influence on LUAD cellular expansion in both laboratory cultures and animal models. Significantly, suppression of B4GALT2 was found to enhance CD8+ T lymphocyte populations and their functional status, thereby potentiating anti-programmed cell death protein 1 immunotherapeutic efficacy in animal studies. This phenomenon was characterized by reduced CD62L+CD8 T lymphocyte levels alongside elevated GZMB+/CD44+/CD69+CD8 T cell populations.

WHAT IS ALREADY KNOWN ON THIS TOPIC

⇒ Lung adenocarcinoma (LUAD) prognosis and treatment efficacy are challenging due to the complex tumor immune microenvironment (TIME). While post-translational modifications are known to influence cancer progression and immune modulation, their role as prognostic markers in LUAD is not fully explored.

WHAT THIS STUDY ADDS

⇒ This study introduces the post-translational modification learning signature (PTMLS), effectively predicting immunotherapy response in LUAD and other cancers. It identifies beta-1,4-galactosyltransferase 2 (B4GALT2) as a novel oncogene linked to immune exclusion and poor prognosis, and elucidates the relationship between PTMLS and the TIME. B4GALT2 knockdown combined with anti-programmed cell death protein 1 therapy significantly enhances antitumor immunity.

HOW THIS STUDY MIGHT AFFECT RESEARCH, PRACTICE OR POLICY

⇒ PTMLS serves as a predictive biomarker for prognosis and immunotherapy suitability, guiding personalized treatment strategies. Targeting B4GALT2 may enhance the efficacy of immunotherapy, which could influence future research directions and clinical decisions, and promote the implementation of biomarker-driven cancer management strategies.

Conclusion The developed PTMLS system represents an effective instrument for individualized prognostic evaluation and immunotherapy stratification in both LUAD and diverse cancer populations. The identification of B4GALT2 as a previously unrecognized oncogenic factor involved in immune exclusion presents a novel therapeutic avenue for LUAD treatment and immunotherapy optimization.

INTRODUCTION

Cancer of the lung represents the primary cause of death among all malignancies.¹ From a histological perspective, pulmonary



neoplasms are categorized into two main groups: non-small cell lung cancer (NSCLC) and small cell lung cancer, with NSCLC comprising approximately 80% of diagnosed cases.² Lung adenocarcinoma (LUAD) emerges as the most frequently encountered subtype within the NSCLC classification. The past several decades have witnessed remarkable advances in detection methods, diagnostic approaches, and therapeutic interventions for NSCLC patients, particularly following the introduction of immune checkpoint blockade therapy, which has demonstrated significant improvements in clinical outcomes.³ Nevertheless, despite these therapeutic innovations, long-term survival metrics remain inadequate, potentially attributable to the intricate interactions occurring between neoplastic tissue and its immunological micro-environment.⁴⁻⁶ Therefore, an imperative exists to elucidate the fundamental molecular pathways associated with unfavorable outcomes in LUAD patients, while simultaneously developing dependable molecular stratification systems capable of both prognostic assessment and therapeutic decision-making in the context of personalized immunotherapy for LUAD management.

Post-translational modifications (PTMs) regulate protein function, expression, and molecular interactions by altering protein properties and stability.^{7,8} Our study examines 20 types of PTMs, including various acylations (acetylation, succinylation, malonylation, crotonylation, β -hydroxybutyrylation, lactylation, palmitoylation, myristoylation), phosphorylation, protein conjugations (SUMOylation, NEDD8ylation, ISGylation, ATG8ylation, FAT10ylation, UFMylation), and other modifications (methylation, glycosylation, biotinylation, S-nitrosylation, ubiquitination/deubiquitination). PTMs have emerged as crucial regulators in cancer biology, particularly in metabolic reprogramming and immune responses.^{9,10} Phosphorylation controls tumor cell behavior through MAPK pathways,¹¹ while ubiquitination manages protein degradation and cellular processes via UPS or lysosomal pathways.^{12,13} In LUAD, deubiquitinases like USP7 influence antitumor immunity by reprogramming tumor-associated macrophages.¹⁴ Several PTMs specifically modulate immune responses: succinylation affects T-cell function through ZAP70 modification,¹⁵ lactylation correlates with immune evasion in cancer,¹⁶ and glycosylation stabilizes PD-L1 expression by preventing its degradation.¹⁷ PTM-mediated regulation of immune checkpoint molecules impacts immunotherapy outcomes.¹⁸ Evidence shows that multiple PTMs participate in immune regulation across various cancers, including NSCLC, thereby influencing tumor immune evasion and treatment resistance.¹⁹

Nevertheless, a comprehensive understanding of the relationship between PTMs and LUAD remains elusive, and the connection between PTMs and alterations in the immune microenvironment requires more detailed investigation. To bridge these knowledge gaps, we integrated 20 types of PTMs in an attempt to identify biomarkers for immunotherapy in LUAD. Leveraging machine learning algorithms, we introduced a novel metric

termed post-translational modification learning signature (PTMLS) to predict therapeutic efficacy and prognosis in LUAD. The investigation revealed that PTMLS demonstrated exceptional efficacy in predicting clinical outcomes among LUAD patients, thereby establishing a robust framework for risk stratification and immunotherapeutic decision-making in both LUAD and diverse cancer populations. Within the PTMLS framework, beta-1,4-galactosyltransferase 2 (B4GALT2) was characterized as an essential molecular component, emerging as a previously undescribed oncogenic factor implicated in immune exclusion mechanisms, thus presenting a novel therapeutic target for LUAD treatment optimization and immunotherapy enhancement.

METHOD

Multi-source data integration

The foundational training data were obtained from The Cancer Genome Atlas (TCGA) portal, encompassing transcriptomic profiles, copy number variations, mutational landscapes, H&E histological preparations, and clinical documentation for LUAD. Model validation incorporated six independent transcriptome collections: GSE13213²⁰ involving 117 cases, GSE26939²¹ involving 115 cases, GSE29016²² involving 39 cases, GSE30219²³ involving 85 cases, GSE31210²⁴ involving 226 cases, and GSE42127²⁵ involving 133 cases. For immunotherapy response evaluation, multiple clinical repositories were analyzed: three LUAD-specific immunotherapy collections: OAK²⁶ involving 257 cases, POPLAR²⁷ involving 59 cases, and NG²⁸ involving 47 cases; four NSCLC data series: GSE126044²⁹ involving 16 cases, GSE166449³⁰ involving 22 cases, GSE207422³¹ involving 24 cases, and GSE135222³² involving 27 cases. Additional validation incorporated pan-cancer immunotherapy collections, including three melanoma repositories: GSE91061,³³ phs000452,³⁴ and GSE100797³⁵; a glioma collection: PRJNA482620³⁶; and clear cell renal cell carcinoma data: Braun_2020.³⁷ Pan-cancer validation used a comprehensive collection of 21 tumor types accessed through UCSC Xena. Single-cell analyses were performed using the GSE207422,³¹ encompassing 15 specimens. Post-translational modification-related genes (PTMRGs) were systematically curated through comprehensive literature examination. Data harmonization protocols included transcripts per million normalization, batch effect mitigation using the "combat" function (sva R package³⁸), logarithmic transformation procedures, and Principal Component Analysis (PCA) for batch effect evaluation. Comprehensive dataset characteristics and PTMRGs documentation are detailed in online supplemental tables S1 and S2.

Identification and evaluation of a PTMLS

The limma R package facilitated PTMRGs expression profiling between tumor and adjacent normal tissues, with differentially expressed genes meeting the criteria of FDR <0.05 and $|\log_2FC|>1$. Prognostically relevant genes were

subsequently identified through univariate Cox regression analysis in the LUAD cohort. Similar to previous studies,³⁹ the construction of an optimal PTMLS involved an extensive computational framework integrating 10 machine learning methodologies: stepwise Cox regression analysis, Lasso regression, Ridge algorithm, plsRcox approach, CoxBoost methodology, RSF computation, GBM analysis, Enet calculation, SuperPC method, and survival-SVM modeling. This integrated analytical pipeline, incorporating 10-fold cross-validation protocols, was designed to generate a signature maximizing the C-index value. The signature's discriminative capability underwent validation through receiver operating characteristic (ROC) analysis and principal component assessment. To position our signature within the existing research landscape, we performed an extensive evaluation against contemporary LUAD prognostic models. Our analysis encompassed 98 established signatures, spanning both lncRNA and mRNA-derived predictive frameworks. The comparative assessment used C-index measurements to ensure objective performance evaluation across all models.

Mechanistic and pathway exploration

The biological implications of PTMRGs were systematically investigated using the “clusterProfiler” package.⁴⁰ Following Entrez ID conversion, functional annotation encompassed both GO and KEGG pathway analyses, with a significance threshold set at adjusted p<0.05. Mechanistic insights were further expanded through GSVA methodology, with particular focus on immune-related processes and immunotherapy response pathways, building on established analytical frameworks.^{41 42} The investigation was enhanced by incorporating MSigDB-derived pathway collections, enabling comprehensive characterization of PTMRGs-associated biological networks.

Genetic alterations and immune landscape analysis

Genomic aberration analysis was conducted using GISTIC 2.0, with emphasis on recurrent amplifications and deletions. We quantified tumor mutational burden (TMB) using the “maf-tools” R package. Immunotherapy response prediction and TIDE scoring across PTMLS subgroups were performed using the TIDE computational framework (<http://tide.dfci.harvard.edu/>). To elucidate the immunological landscape of LUAD patients and identify potential immunotherapy responders, we accessed the Cancer Immunome Atlas (<https://tcia.at/home>) for immunophenoscores. The ssGSEA algorithm was employed to evaluate both lymphocyte presence and immunological pathway activation within neoplastic tissues. For a comprehensive immunological profile of TCGA specimens, we consulted the TIMER2.0 database, which integrates results from multiple analytical approaches (as detailed in online supplemental table S3). Furthermore, we harnessed the diverse immunological deconvolution algorithms available in the IOBR

package^{39 43} to estimate intratumoral immune cell populations.

Computational pipeline for single-cell transcriptome analysis

The raw transcriptomic data matrix underwent quality control and normalization using the Seurat R toolkit (V.4.2.0).⁴⁴ Transcripts detected in a minimum of 10 cells per specimen were retained for further scrutiny. Cellular entities were filtered based on stringent quality metrics: exclusion of cells expressing >5000 or <200 genes, and those with mitochondrial transcript proportion exceeding 10% of total unique molecular identifiers. Inter-sample batch effects were mitigated through the application of the harmony algorithm. PCA was applied to reduce dimensions of highly variable genes, followed by t-SNE analysis of the top 30 principal components to visualize gene expression patterns. Differential gene expression analysis within distinct cellular subsets was conducted using the “FindAllMarker” utility. Cell-type annotation was performed based on established lineage-specific molecular signatures from peer-reviewed literature.⁴⁵

Intercellular signaling network analysis

To elucidate the intricate web of cellular crosstalk, we employed the CellChat algorithm^{39 46} for deciphering intercellular communication patterns within the tumor ecosystem. This computational approach integrates transcriptomic profiles to unveil differential signaling modules across diverse cell populations. The analysis was conducted using the standard CellChat protocol, with the default CellChatDB serving as the reference repository for ligand-receptor interactions. By identifying cell type-specific molecular signatures, we inferred potential cellular dialogs based on the overexpression of signaling molecules. Enhanced ligand-receptor interactions were postulated when either the ligand or its cognate receptor exhibited elevated expression levels in particular cellular subsets.

Cell Culture and Lentiviral Transfection

A549 and H1299 LUAD cells were sourced from the Institute of Biochemistry and Cell Biology (Shanghai, Chinese Academy of Sciences). Cell maintenance was performed in RPMI 1640 media containing 10% FBS and standard antibiotics (penicillin 100 U/mL, streptomycin 100 mg/mL). Human and mouse B4GALT2 lentiviral particles were purchased from Shanghai Genechem Co., Ltd. (Shanghai, China). Lentiviral infection was performed according to the manufacturer's instructions. The experimental design involved cell seeding in 6-well plates and viral transfection. Knockdown efficiency was monitored via qRT-PCR analysis. The primer sequences targeting B4GALT2 and reference gene GAPDH are provided in online supplemental table S4.

Assessment of clonogenic potential

To evaluate clonogenic capacity, 5×10³ cells were inoculated per well in 6-well culture plates. Cells were maintained in a standard growth medium, which was

replenished after 7 days. Following a 14-day incubation period, allowing for sufficient colony development, the cultures underwent fixation with methanol for a quarter-hour. Subsequently, cellular staining was performed using a 0.1% crystal violet solution (Sigma) for 30 min. Quantification of clonogenic ability was achieved by enumerating the resultant stained colonies.

Construction of an in-house LUAD cohort

Formalin-fixed paraffin-embedded specimens were retrieved from the Pathology Department archives at Tianjin Medical University Cancer Institute and Hospital. Pathological assessment verified LUAD diagnosis in all cases. These specimens were collected from treatment-naïve patients who had not received any form of radiotherapy, chemotherapy, or molecular-targeted interventions before surgical resection. Detailed demographic and clinical parameters of the study population are summarized in online supplemental table S5.

Multiplexed immunohistochemistry analysis

A validated multiplexed immunohistochemistry protocol^{39–47} was implemented to examine the spatial distribution patterns between B4GALT2 and immune cell populations, with concurrent DAPI nuclear visualization. The optimized antibody panel included B4GALT2 (ProteinTech, 20330-1-AP, 1:200), CD8A (Abcam, ab217344, 1:2000), and CD20 (Abcam, ab64088, 1:100). For immunohistochemical analysis, LUAD tissue specimens underwent sequential processing steps, including xylene-mediated deparaffinization and ethanol gradient rehydration. Endogenous peroxidase activity was neutralized using 3% hydrogen peroxide solution, followed by non-specific binding blockade with 5% goat serum. Tissue sections were subjected to overnight incubation with B4GALT2 primary antibody (1:50, ProteinTech, 20330-1-AP) at 4°C, followed by 30 min exposure to HRP-conjugated secondary antibodies. Visualization was achieved through DAB chromogen development and hematoxylin nuclear counterstaining. Staining interpretation was performed independently by two pathologists, with B4GALT2 expression quantified using the H-score algorithm. Immune contexture classification was established based on CD8+ T cell infiltration patterns, yielding three distinct phenotypes: inflamed, excluded, and desert.

Mouse model for immune response assessment

Experimental C57BL/6 mice were acquired from Gempharmatech (Jiangsu, China). The xenograft model was established by subcutaneous administration of sh-B4galt2 LLC cells (2×10^5 cells/100 µL PBS). Therapeutic intervention commenced on tumors reaching 100 mm³. The study groups were administered either anti-programmed cell death protein 1 (PD-1) monoclonal antibody (BioXcell, BE0146) or isotype-matched IgG control (BioXcell, BE0089) via intraperitoneal route. Each dose consisted of 100 µg antibody in 100 µL D-PBS.

Tumor measurements were documented bi-weekly, with volume calculations performed using the formula: $0.5 \times \text{length} \times \text{width}^2$. Terminal tumor mass was recorded at study completion.

Analysis of tumor-infiltrating immune populations by flow cytometry

Tumor specimens harvested from C57BL/6 mice underwent enzymatic dissociation using collagenase IV/DNase I treatment (2-hour incubation), followed by mechanical filtration through 70 µm mesh to generate single-cell preparations. Leukocyte populations were enriched via Percoll density gradient centrifugation (40%/70% interface). Isolated cells were exposed to a leukocyte activation cocktail (4 hours) for cytokine assessment, with subsequent Fc receptor blockade using anti-CD16/CD32 antibodies. Immunophenotyping was performed using a comprehensive panel of fluorochrome-labeled antibodies, including CD45 (30-F11) for leukocyte identification, T-cell markers CD3ε (17A2) and CD8α (53-6.7), and activation markers CD44 (IM7), CD62L (MEL-14), and CD69 (H1.2F3). Following membrane permeabilization procedures, intracellular GZMB detection was achieved using specific monoclonal antibodies (QA16A02). Multi-parameter analysis was conducted on a BD FACS Canto II platform with subsequent data processing using FlowJo analytical software.

Statistical analyses

Statistical evaluations were conducted using R V.4.2.0. Survival analyses across subgroups used Kaplan-Meier curves with significance determined by log-rank statistics. For quantitative data comparisons, Wilcoxon tests or Student's t-tests were applied as appropriate. Discrete variable associations were examined through χ^2 methodology or Fisher's exact testing when indicated. Multiple comparison corrections employed the FDR approach. Variable relationships were quantified using Pearson's correlation coefficients. Statistical significance was established at $p < 0.05$ (two-tailed).

RESULT

Investigation of PTM-associated markers

PTM-dependent regulation of the TME by malignant cells represents a critical challenge in contemporary oncology, particularly in immune response modulation. This investigation aimed to characterize LUAD-specific PTM markers through comprehensive bioinformatic analysis. The research methodology is outlined in figure 1. Following batch effect elimination between GTEx and TCGA datasets, differential expression analysis identified PTMRGs distinguishing LUAD from normal tissue (figure 2A). Survival correlation analysis revealed 31 prognostically significant PTMRGs ($p < 0.05$, online supplemental table S6, figure 2B). Functional annotation through GO and KEGG pathways demonstrated these genes' involvement in ubiquitination, histone modification, and glycosylation

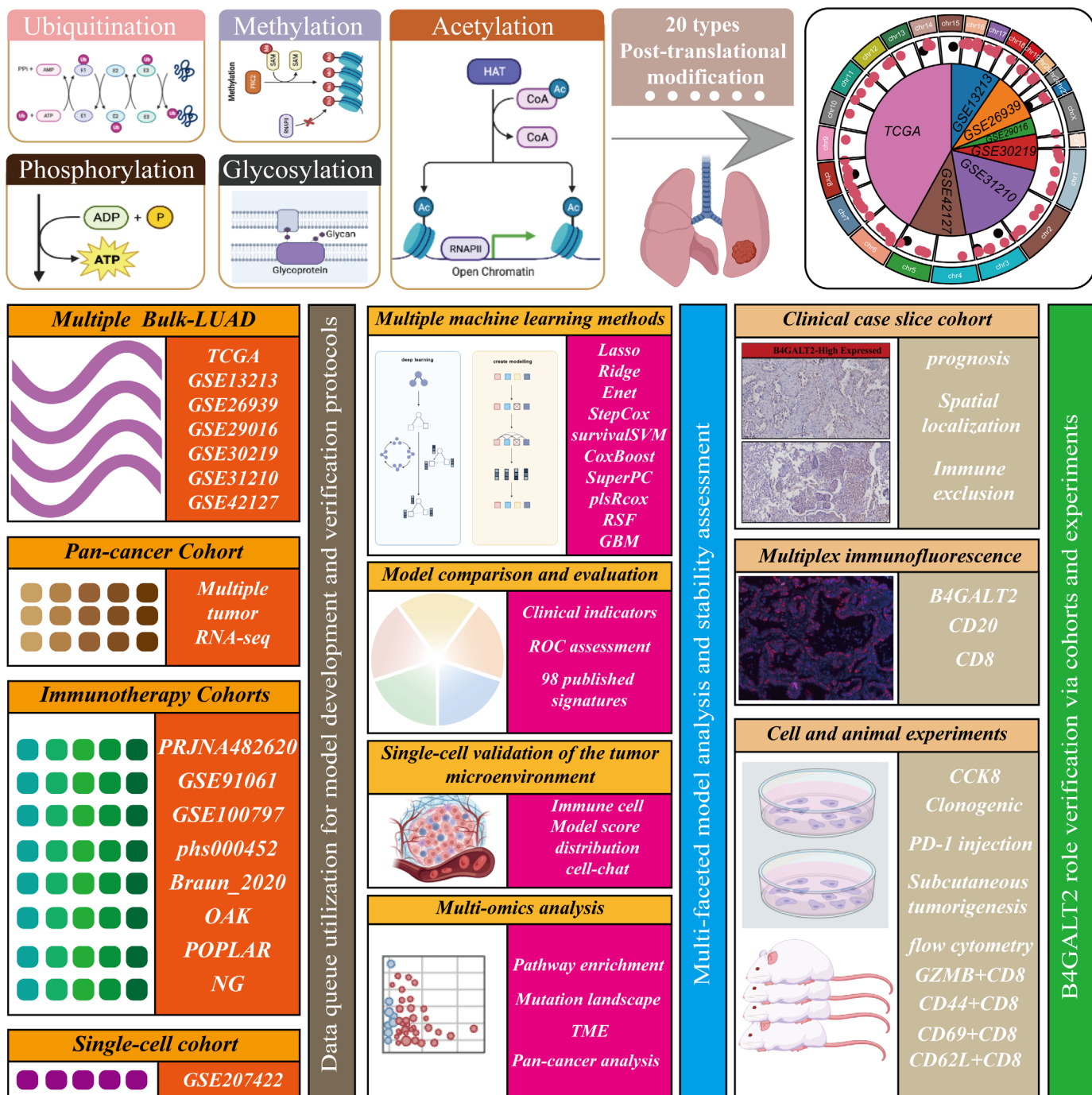


Figure 1 Flowchart of PTMLS development and validation in LUAD. PTMLS was constructed using 20 post-translational modification-related genes and validated across seven multicenter LUAD cohorts. The flowchart illustrates PTMLS development, evaluation of its prognostic and immunotherapy predictive value, identification of B4GALT2 as a key gene, and investigation of B4GALT2's role in creating a “desert-like” tumor microenvironment. In-house cohort samples and in vitro/in vivo experiments further explored B4GALT2's function in immune exclusion and LUAD proliferation. B4GALT2, beta-1,4-galactosyltransferase 2; LUAD, lung adenocarcinoma; PTMLS, post-translational modification learning signature.

cascades (figure 2C,D). Data harmonization was performed across seven LUAD transcriptome datasets to minimize technical variation (online supplemental figure S1A). ssGSEA analysis comparing TCGA tumor samples with GTEx normal tissues revealed elevated S-nitrosylation activity in neoplastic tissue (figure 2E). Genomic mapping illustrated PTMRG chromosomal distribution and expression patterns (figure 2F), while CNV analysis

documented frequent genomic alterations affecting these loci (figure 2G).

PTMLS: a novel prognostic and immunotherapy response predictor

We constructed a PTMLS incorporating 31 survival-associated PTMRGs through machine learning integration. Model development used TCGA data, with validation

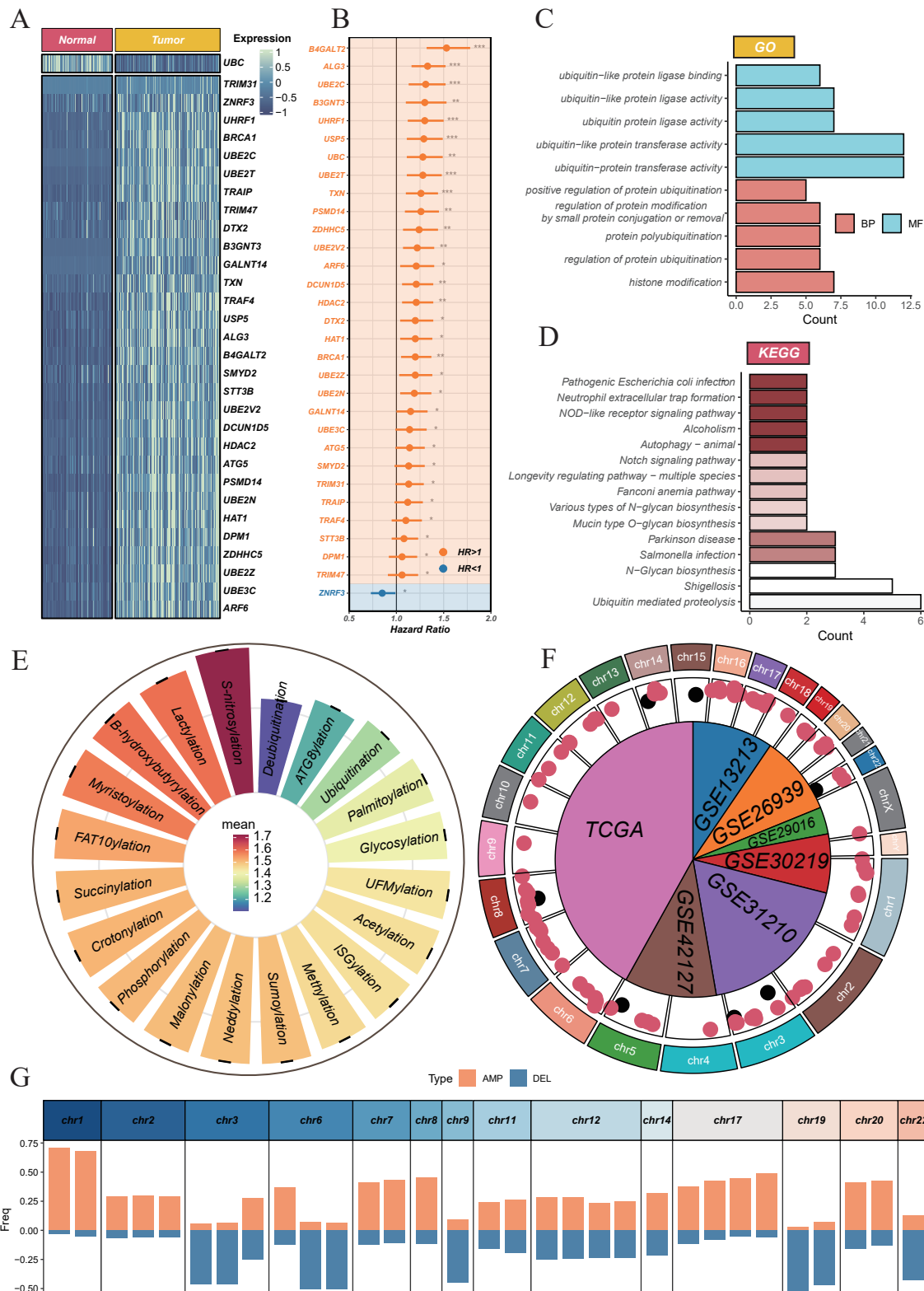


Figure 2 Characterization and evaluation of PTM-associated genes in prognosis. (A) Assessment of PTMRGs expression alterations between neoplastic and normal pulmonary specimens. (B) Survival correlation analysis was performed to detect PTMRGs with prognostic significance. (C,D) Pathway enrichment investigation was conducted using GO and KEGG databases to elucidate biological functions of prognostic PTMRGs. (E) Quantitative comparison of PTM-specific ssGSEA scores was executed between neoplastic and non-neoplastic samples. (F) Genomic distribution of prognostic PTMRGs was mapped, with red indicators signifying elevated expression in neoplastic tissue ($\log_2(FC)$ values correlate with radial position), while black indicators denote the inverse pattern. The central diagram illustrates LUAD cohorts used in model development. (G) Genomic positioning and CNV status of prognostic PTMRGs were documented. LUAD, lung adenocarcinoma; PTM, post-translational modification; PTMRGs, post-translational modification-related genes.

across six independent GEO cohorts. Algorithm selection prioritized optimal mean C-index performance across validation sets, identifying Stepcox (both)+SuperPC as the superior approach (figure 3A). PTMLS demonstrated robust prognostic stratification capability across all study cohorts (figure 3B–H), with elevated scores correlating with adverse outcomes. The model's predictive utility extended to immunotherapy response, as validated in three LUAD-specific cohorts (online supplemental figure S1B, figure 3I–K) and five diverse cancer datasets (online supplemental figure S1C–H). Lower PTMLS scores are consistently associated with enhanced immunotherapy outcomes. Analysis of four NSCLC cohorts with documented treatment responses (figure 3L) revealed significantly reduced PTMLS scores among responders compared with non-responders (figure 3M–P). Complementary evaluation using TCIA-derived Immunophenotype Scores confirmed superior immunotherapy suitability (PD-1, CTLA-4, or combination therapy) in the low PTMLS group (figure 3Q–T), suggesting enhanced tumor immunogenicity. The model's consistent performance across multiple cancer types establishes PTMLS as a potential pan-cancer biomarker for immunotherapy response prediction.

Clinical validation of PTMLS prognostic performance

Comparative analysis across seven independent cohorts demonstrated PTMLS's superior predictive accuracy over conventional clinical parameters, including age, gender, staging, and EGFR status, as reflected by enhanced C-index values (figure 4A). PCA visualization based on PTMLS component genes revealed distinct clustering between high and low-score groups, indicating fundamental biological differences (figure 4B). ROC analysis confirmed PTMLS's robust prognostic capability, achieving area under the curve values exceeding 0.65 for 1-, 3-, and 5-year survival predictions across datasets (figure 4C). When benchmarked against 98 established LUAD signatures, PTMLS consistently demonstrated optimal performance with superior C-index scores (figure 4D). Clinical correlation analysis revealed significant associations between elevated PTMLS scores and increased mortality, advanced T/N staging, and overall disease progression (online supplemental figure S2A). Expression profiling showed uniform upregulation of model genes in high PTMLS cases, with UBE2C notably overexpressed across multiple cancer types (online supplemental figures S2B). Pan-cancer PTMLS distribution analysis (online supplemental figure S3A) and pathway enrichment studies identified significant correlations with proliferation-associated pathways, including MYC targets, mTOR signaling, and cell cycle regulation (online supplemental figure S3B), suggesting PTMLS's mechanistic involvement in tumor progression through cell growth modulation.

Genomic alterations and their relationship with PTMLS status

Similar to our previous investigation in LUAD,³⁹ genomic stability analysis revealed distinct patterns between

PTMLS subgroups (online supplemental figure S4A,B), with high PTMLS cases showing increased chromosomal aberrations. Mutational profiling (online supplemental figure S4C) identified elevated TMB in the high PTMLS group, predominantly affecting TP53, TNN, MUC16, CSMD3, and RYR2 genes, which regulate the cell cycle, matrix organization, mucus production, neural development, and calcium signaling. CNV analysis (online supplemental figure S4D–G) confirmed enhanced genomic instability in high PTMLS tumors through frequent chromosomal alterations. While PTMLS demonstrated a positive correlation with TMB ($r=0.36$, $p<0.05$, online supplemental figure S5H,I), survival analysis revealed an unexpected pattern: patients with low TMB but high PTMLS showed the poorest outcomes (online supplemental figure S4J).

PTMLS impact on cellular interactions and immune microenvironment

The single-cell analysis identified 11 distinct cellular populations through dimensional reduction and marker gene profiling (online supplemental figure S5A,B). Cell-type specific expression mapping revealed preferential B4GALT2 expression in tumor cells, while ZDHHC5 and UBE2V2 predominantly marked immune populations (online supplemental figure S5C). PTMLS stratification demonstrated an inverse correlation between score and immune cell abundance (online supplemental figure S5D), suggesting its regulatory role in TME composition. Intercellular communication analysis revealed enhanced signaling network activity in PTMLS_high populations (online supplemental figure S5E–G), with notable upregulation of immunosuppressive pathways including TGF β , SPP1, and VEGF (online supplemental figure S5H, I). PTMLS_high cells exhibited amplified bidirectional signaling capabilities, showing enhanced signal transmission and reception (online supplemental figure S5J). These findings indicate PTMLS's dual role in promoting tumor cell prevalence and establishing an immunosuppressive microenvironment through enhanced cellular communication networks.

PTMLS as a determinant of tumor immune landscape

Comprehensive immune profiling revealed distinct patterns between PTMLS subgroups. Low PTMLS tumors demonstrated enhanced infiltration of CD8+ T cells, B cells, and NK cells ($p<0.05$) (figure 5A), suggesting augmented antitumor immunity. ssGSEA analysis confirmed this pattern, showing elevated immune cell presence and activated type II interferon response and antigen presentation pathways in low PTMLS cases (figure 5B). Immune regulatory gene analysis revealed differential expression patterns: low PTMLS tumors upregulated MHC class II and costimulatory molecules, while high PTMLS cases showed MHC class I activation, including TAP1/TAP2 (figure 5C). The TIDE algorithm predicted superior immunotherapy response potential in low PTMLS patients (figure 5D). ESTIMATE analysis

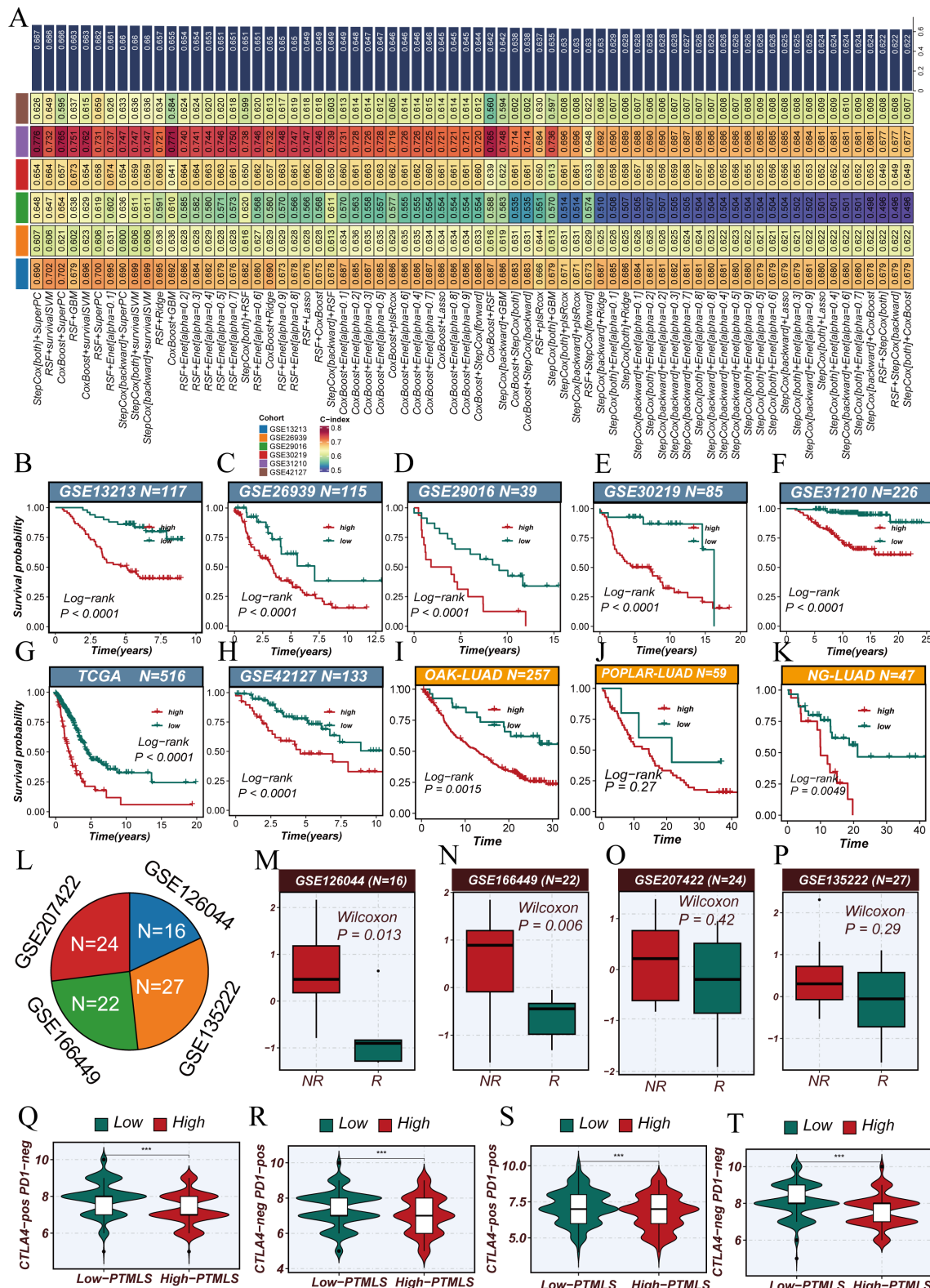


Figure 3 Development and clinical assessment of PTMLS via computational approaches. (A) PTMLS was established through diverse machine learning algorithms, with heatmap values indicating prognostic C-indices; the upper histogram demonstrates mean C-index across datasets. (B–H) PTMLS demonstrated significant prognostic stratification capacity across seven LUAD cohorts, with favorable outcomes observed in low PTMLS subjects. (I–K) PTMLS prognostic utility was validated in LUAD immunotherapy populations. (L–P) PTMLS levels were examined between therapeutic response groups across four NSCLC cohorts, consistently revealing elevated PTMLS in non-responding subjects. (Q–T) IPS predictions were generated for TCGA-LUAD cases via TCIA, demonstrating enhanced IPS scores and immunotherapy responsiveness in low PTMLS populations. IPS, immunophenoscores; LUAD, lung adenocarcinoma; NSCLC, non-small cell lung cancer; PTM, post-translational modification; PTMLS, post-translational modification learning signature.

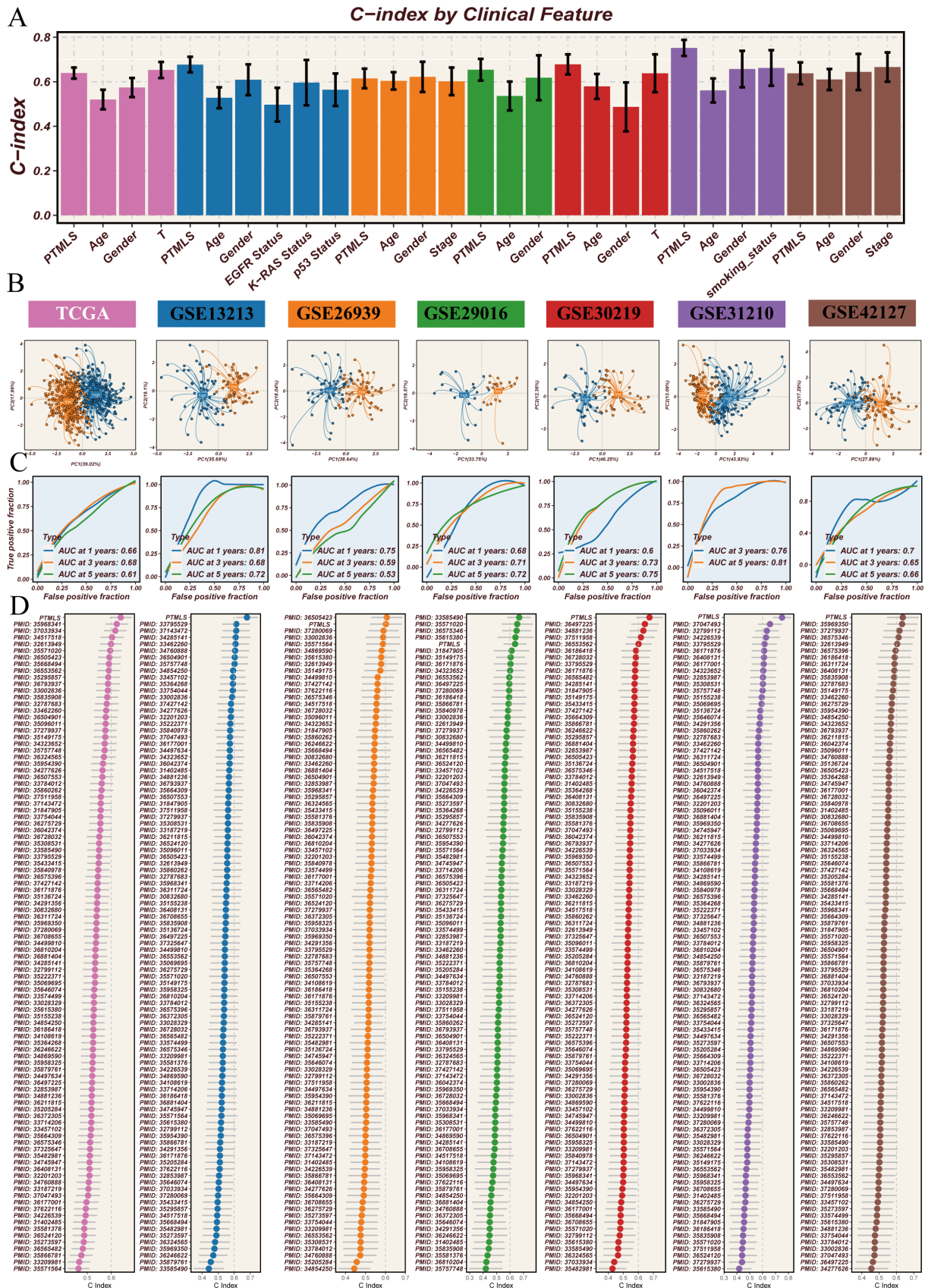


Figure 4 Evaluating PTMLS as a prognostic tool in LUAD. (A) PTMLS performance relative to established clinical indicators. (B) Two-cluster separation in Principal Component Analysis of model gene expression across seven datasets (blue: high PTMLS, orange: low PTMLS). (C) Prognostic accuracy assessment via receiver operating characteristic curves for seven datasets. (D) Comparative analysis of PTMLS against published LUAD-specific signatures, highlighting PTMLS's enhanced predictive power. LUAD, lung adenocarcinoma; PTMLS, post-translational modification learning signature.

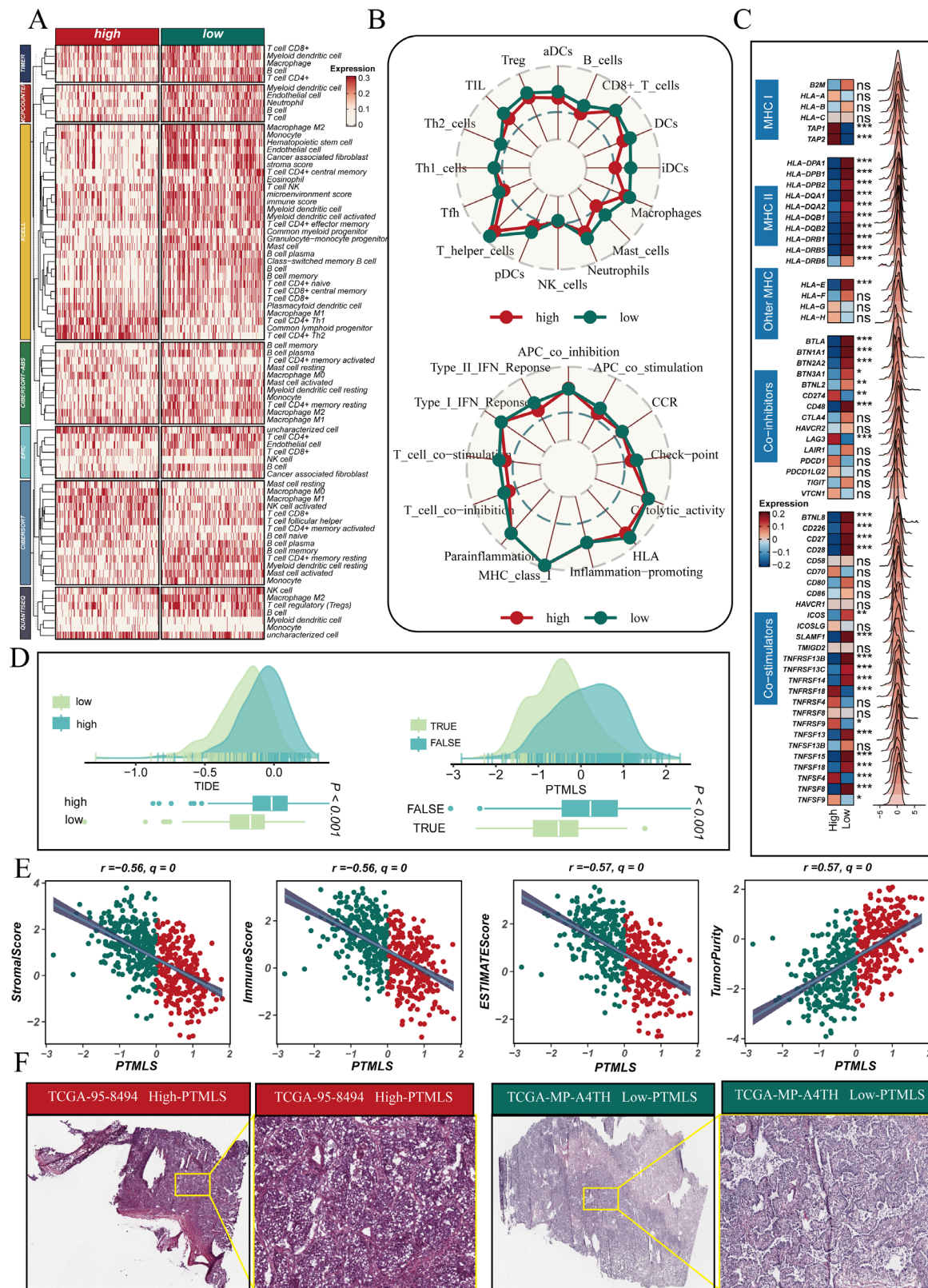


Figure 5 Immunological and genomic distinctions among PTMLS subgroups. (A) Quantitative evaluation of immune cell distribution variations between high versus low MPCDS populations was conducted via the TIMER2.0 platform. (B) ssGSEA methodology was employed to examine immune infiltration patterns and pathway activation status across subgroups. (C) Differential expression investigation of immune modulatory molecules between subgroups was performed. (D) TIDE platform was used to assess therapeutic response probability and TIDE score variations among PTMLS subgroups. (E) Estimate R package was applied to analyze associations between PTMLS and immune signature scores. (F) Histological and genomic examination was conducted to evaluate immune infiltration patterns across PTMLS subgroups, with representative TCGA-LUAD sections displayed. PTMLS, post-translational modification learning signature.

demonstrated a positive correlation between PTMLS and tumor purity, with an inverse relationship to immune scores (figure 5E). Histological validation using TCGA H&E slides confirmed increased lymphocytic infiltration in low PTMLS tumors (figure 5F). These findings establish PTMLS as a potential biomarker for immune response prediction and therapeutic stratification.

B4GALT2: a key determinant in LUAD progression and immune response

Analysis revealed a strong correlation between B4GALT2 expression and PTMLS scores ($r=0.82$, $q=0$) (figure 6A), establishing B4GALT2 as a central component of the PTMLS model. Elevated B4GALT2 expression consistently predicted poor survival across multiple cohorts (HR=1.62, 95% CI 1.36 to 1.92, log-rank $p=3.9e-08$) (figure 6B–H). HPA immunohistochemistry confirmed B4GALT2 overexpression in tumor versus normal lung tissue (figure 6I–L). Clinical correlation studies demonstrated inverse relationships between B4GALT2 levels and both MPR (figure 6M) and CD8A expression (LUAD-TCGA: $R=-0.25$, $p=1.4e-05$; LUAD-Atezo: $R=-0.2$, $p=3.2e-06$) (figure 6N,O). Expression analysis across treatment groups showed the lowest B4GALT2 levels in MPR cases and the highest in treatment-naïve patients (figure 6P). Tumor immune microenvironment characterization revealed distinct immune infiltration patterns associated with B4GALT2 expression (figure 6Q), showing negative correlations with immune and ESTIMATE scores but positive associations with tumor purity. These findings establish B4GALT2 as a novel prognostic marker and immune response modulator in LUAD.

B4GALT2 and CD8+ T cell distribution: clinical implications

Analysis of our institutional cohort revealed distinct CD8+ T cell infiltration patterns and their prognostic significance. Clinical data demonstrated increased mortality and lymphatic spread in desert phenotype cases (figure 7A). Based on CD8+ T cell distribution, we classified samples into Desert, Excluded, and Inflamed phenotypes, with representative histological images shown in figure 7B. Survival analysis confirmed significantly reduced DFS and OS in Desert phenotype patients (log-rank test $p<0.0001$) (figure 7C,D). B4GALT2 expression showed phenotype-specific variation, with highest levels in Desert and lowest in Inflamed cases (Kruskal-Wallis test, $p<0.05$) (figure 7E). IHC-based B4GALT2 stratification (figure 7F) revealed shortened survival in high expression cases (log-rank test $p=0.033$) (figure 7G), establishing B4GALT2 as a marker of immunologically cold tumors with poor outcomes.

B4GALT2's role in immune regulation and treatment response

Expression analysis revealed inverse relationships between B4GALT2 and key immune components, including chemokines (CXCL13, CCL5, CCL14), MHC molecules, and immune regulatory factors (figure 8A, online supplemental figure S6A). Pathway analysis demonstrated a positive correlations with cell cycle regulators (E2F targets,

G2M checkpoint) and EMT, while showing negative associations with immune processes including antigen presentation and lymphocyte recruitment (online supplemental figure S6B). Multi-color immunofluorescence confirmed spatial exclusion between B4GALT2 expression and CD8+ T/CD20+ B cell infiltration (figure 8B). Functional studies in A549 and H1299 cells showed B4GALT2 knockdown significantly suppressed proliferation, as evidenced by CCK8 and colony formation assays (figure 8C–G). In vivo experiments using C57BL/6 mice and LLC cells demonstrated enhanced antitumor effects when combining B4GALT2 knockdown with PD-1 blockade (figure 8H–J), with the combination therapy showing superior tumor growth inhibition compared with either treatment alone.

B4GALT2 inhibition potentiates anti-PD-1 response through T cell activation

Flow cytometry analysis unveiled how B4GALT2 knockdown reshapes the immune landscape to enhance immunotherapy efficacy. Most strikingly, the combination of B4GALT2 suppression and PD-1 blockade (shB4galt2+anti-PD1) maximized the presence of effector immune cells, particularly evident in both total CD8+ T cells and their activated subsets (CD44+/CD69+/GZMB+) (figure 9A,B). This enhanced activation state was further supported by the corresponding decrease in naive CD8+ T cells (CD62L+) compared with control groups (shNC), indicating successful conversion from resting to effector status. Together, these findings reveal a mechanistic basis for the synergistic effect: B4GALT2 inhibition appears to create a permissive environment for PD-1 blockade by promoting T cell activation and effector function.

DISCUSSION

As one of the most prevalent cancers globally, lung cancer, particularly LUAD, has been extensively studied in terms of its development and immunotherapy. PTMs play a pivotal role in tumor progression. For instance, oncogenic protein arginine methyltransferase 5 promotes colorectal cancer metastasis by methylating SMAD4 R361, thereby activating TGF- β signaling.⁴⁸ Lactylation can drive hepatocellular carcinoma growth and dissemination by modulating tumor cell metabolism.⁴⁹ Phosphorylated cyclin-dependent kinase 5 is essential for pancreatic cancer cell metastasis, angiogenesis, and immune evasion.⁵⁰ Additionally, in bladder cancer, modulating the ubiquitination of E3 ubiquitin ligase compounds has been shown to enhance immunotherapy efficacy.⁵¹ These previous studies on PTMs in other cancers provide important references for understanding the impact of PTMs on LUAD. Our systematic investigation of PTMs revealed their crucial role in LUAD progression. By integrating data from 1231 LUAD patients across seven international cohorts, we developed PTMLS—a robust computational framework that captures the prognostic significance of 20 key PTMs. The model's clinical utility extends beyond LUAD, as validated across 12

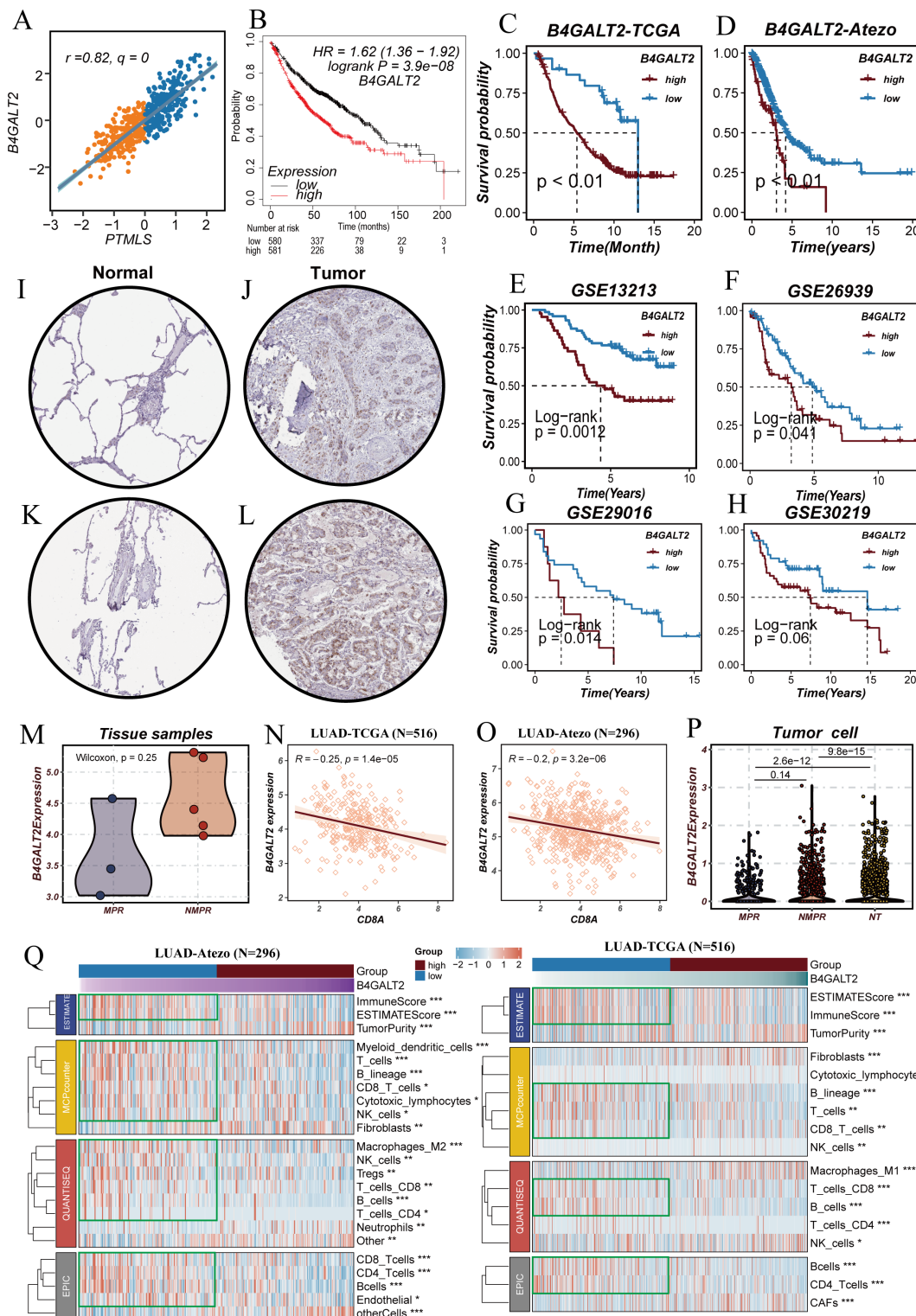


Figure 6 B4GALT2 expression patterns and clinical significance in LUAD. (A) Statistical assessment of B4GALT2 and PTMLS score correlation was executed. (B) The KM plotter platform was used to evaluate B4GALT2's prognostic value in LUAD patients. (C-H) Survival significance of B4GALT2 was validated across six independent cohorts, encompassing one immunotherapy and five conventional LUAD populations. (I-L) HPA database-derived B4GALT2 immunostaining demonstrated elevated expression in neoplastic tissues. (M) Single-cell transcriptomic analysis from GSE207422 revealed B4GALT2 expression variations between MPR and NMPR cohorts. N-O. Significant inverse correlation was observed between B4GALT2 and CD8A expression in both TCGA-LUAD and Atezo-LUAD datasets. (P) B4GALT2 expression patterns were compared among MPR/NMPR/NT groups using tumor cells isolated from GSE207422. (Q) Transcriptome-level analysis revealed a progressive reduction in immune cell infiltration (including CD8+, B cells, and NK cells) correlating with increased B4GALT2 expression across both datasets. B4GALT2, beta-1,4-galactosyltransferase 2; LUAD, lung adenocarcinoma; PTMLS, post-translational modification learning signature.

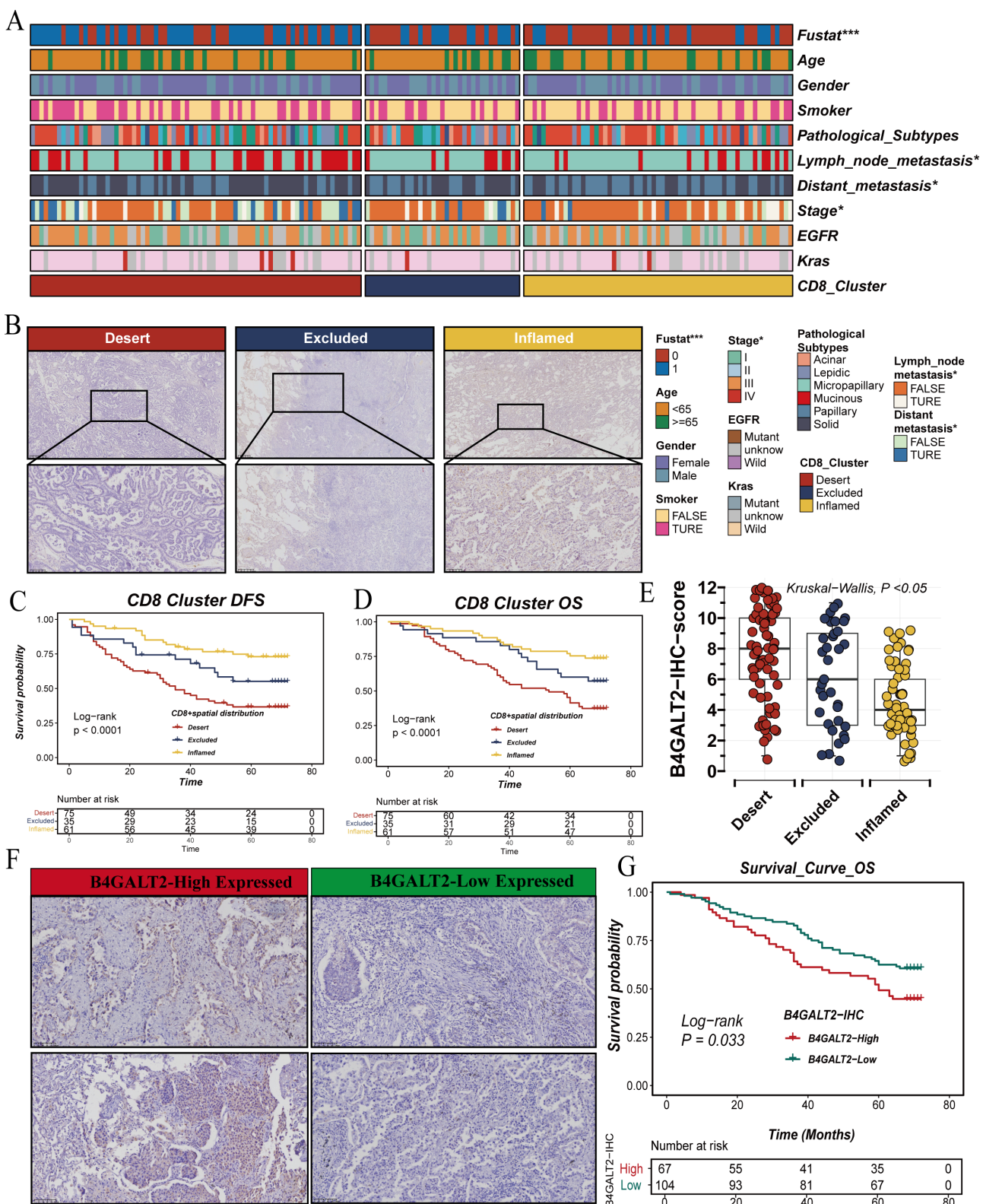


Figure 7 High B4GALT2 expression correlates with worse prognosis and promotes a desert phenotype in the microenvironment. (A) Clinical characteristics of 171 patients from a hospital cohort, divided into three groups: desert, excluded, and inflamed types. (B) Representative immunohistochemistry images of desert, excluded, and inflamed phenotypes. (C, D) Impact of desert, excluded, and inflamed types on OS and DFS in LUAD patients. The inflamed type shows the best prognosis, while the desert type has the worst. (E) Evaluation of B4GALT2 expression differences among desert, excluded, and inflamed groups, with the desert type showing the highest B4GALT2 expression. (F) Representative immunohistochemistry images of high and low B4GALT2 expression. (G) Analysis of B4GALT2's impact on patient prognosis by dividing patients into high and low expression groups based on B4GALT2 expression levels. B4GALT2, beta-1,4-galactosyltransferase 2; DFS, disease-free survival; LUAD, lung adenocarcinoma; OS, overall survival.

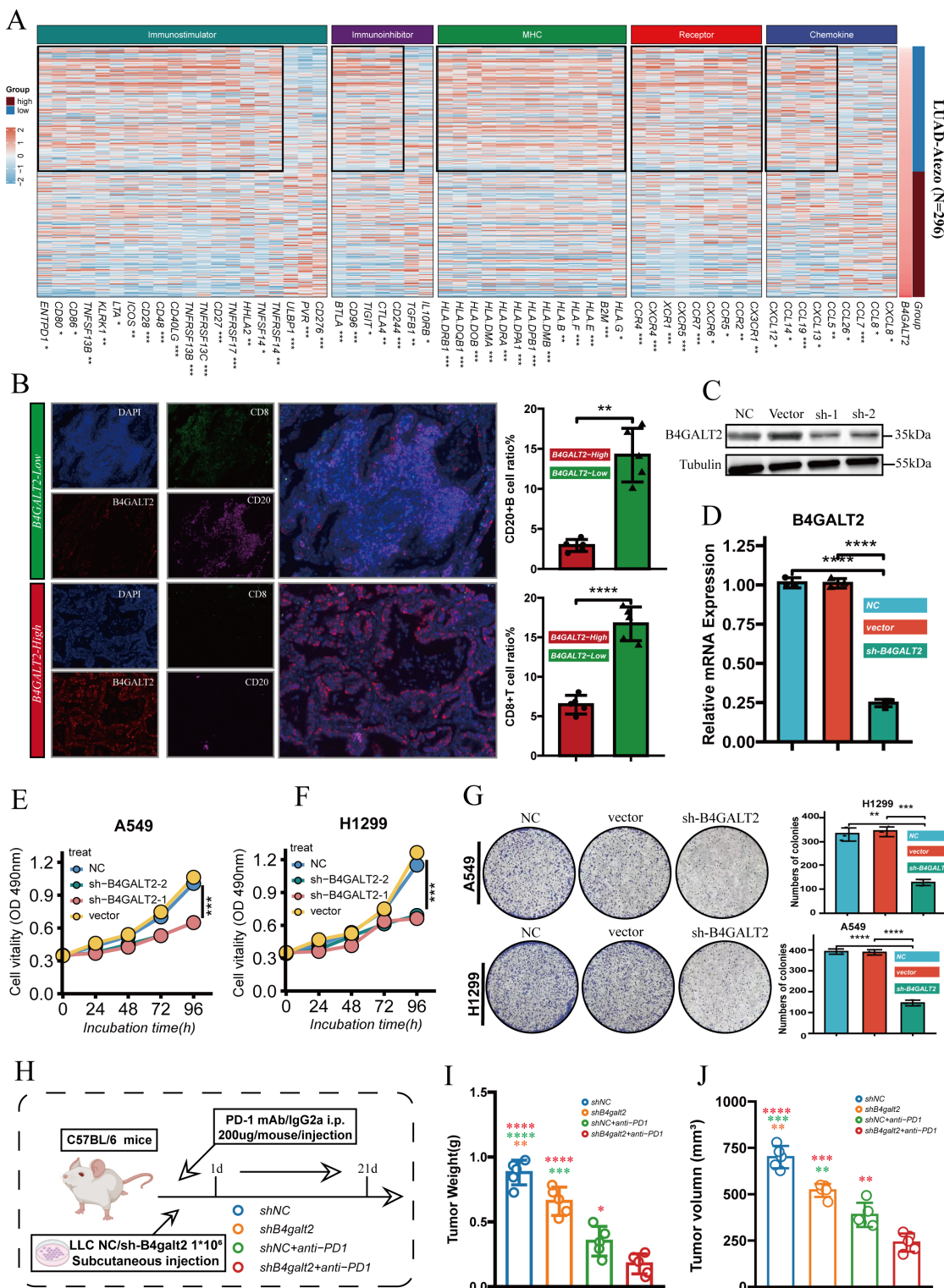


Figure 8 B4GALT2-mediated regulation of immune microenvironment and neoplastic growth. (A) The correlation matrix revealed inverse associations between B4GALT2 levels and immune-related transcripts, with prominent immune gene clusters (highlighted by black margins) exhibiting the strongest negative correlations. (B) The spatial distribution of CD8 and CD20 lymphocytes was visualized via multiplexed immunofluorescence in regions displaying differential B4GALT2 abundance. (C, D) Successful B4GALT2 suppression in LUAD cell lines was validated through immunoblotting and quantitative PCR analyses. (E–G) Cellular viability and colony formation capacity following B4GALT2 manipulation were assessed via CCK8 and clonogenic methodologies. (H) Experimental design involved subcutaneous inoculation of C57BL/6 mice with 1×10^6 sh-B4galt2 or control LLC cells, followed by administration of either PD-1 specific antibody or corresponding IgG2a control. (I) Temporal monitoring of tumor progression across treatment groups demonstrated optimal therapeutic efficacy in the shB4galt2+anti-PD1 cohort, manifesting as significantly attenuated tumor expansion. B4GALT2, beta-1,4-galactosyltransferase 2; LUAD, lung adenocarcinoma; PD-1, programmed cell death protein 1.

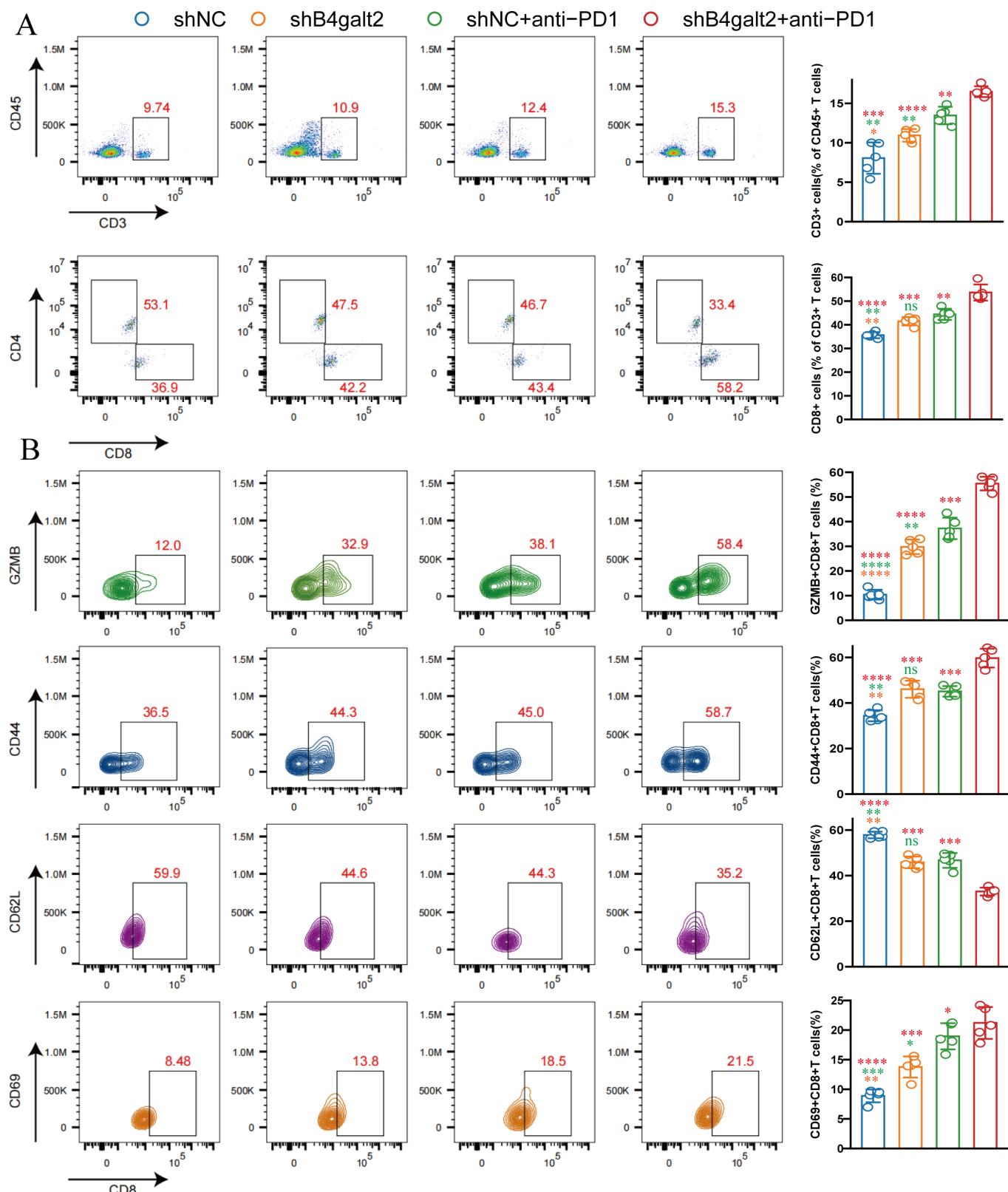


Figure 9 Synergistic enhancement of anti-PD-1 response via B4GALT2 suppression: modulation of CD8+ T cell phenotypes. (A) Flow cytometric analysis demonstrated augmented CD8+ T lymphocyte infiltration following both B4GALT2 suppression and PD-1 blockade, with maximal infiltration observed in the combination therapy cohort. (B) Representative cytometric profiles validated that dual intervention (shB4galt2+anti-PD1) substantially elevated activated CD8+ T cell populations while diminishing naive subset abundance. Technical annotation: GZMB serves as a cytolytic activity indicator, CD44/CD69 function as activation status markers, and CD62L identifies naive populations within CD8+ T lymphocytes; statistical significance: * $p<0.05$, ** $p<0.01$, *** $p<0.001$, **** $p<0.0001$, ns, not significant. B4GALT2, beta-1,4-galactosyltransferase 2; LUAD, lung adenocarcinoma; PD-1, programmed cell death protein 1.



immunotherapy cohorts ($n=1201$) spanning multiple cancer types including NSCLC, melanoma, glioma, and clear cell renal cell carcinoma. Notably, PTMLS demonstrated superior prognostic accuracy compared with 98 existing LUAD signatures, positioning it as a valuable tool for personalizing immunotherapy strategies and optimizing patient outcomes.

B4GALT2, encoded by the B4GALT2 gene, is a member of the β -1,4-galactosyltransferase family and plays a crucial role in the glycosylation process. This process is essential for various cellular functions, including cell recognition, signal transduction, and immune responses. Aberrations in B4GALT2 expression and function have been widely associated with the initiation, development, and progression of various tumors. For instance, upregulation of B4GALT2 has been observed in the cisplatin-resistant ovarian cancer cell line A2780-CP, suggesting its potential involvement in platinum resistance mechanisms.⁵² Furthermore, Srividya Venkitachalam *et al* found that mutations in genes involved in synthesizing N-linked and Core 1-3 O-linked glycans, including B4GALT2, are enriched in colorectal cancer, significantly enhancing tumor cell migration capacity.⁵³ In our study, B4GALT2 emerged as a key gene, showing a significant positive correlation with PTMLS ($r=0.82$, $p<0.05$). PTMLS has been demonstrated to effectively predict outcomes for patients undergoing immunotherapy across various cancer types, with the high PTMLS group exhibiting lower immune activity, indicative of a “cold tumor” phenotype. Our research further elucidated the oncogenic role of B4GALT2 in LUAD. Validation in our in-house cohort confirmed that high B4GALT2 expression is significantly associated with poor prognosis in LUAD patients, particularly in the CD8-deficient phenotype. Multiplex immunofluorescence experiments confirmed the spatial co-localization and exclusion relationship between B4GALT2 and CD8+ T cells and CD20+ T cells, strongly suggesting B4GALT2’s involvement in immune exclusion processes. Knockdown of B4GALT2 in LUAD cell lines (eg, A549 and H1299) significantly impaired cell proliferation, a finding validated both in vitro and in vivo. More importantly, flow cytometry experiments revealed that B4GALT2 inhibition not only increased the quantity of CD8+ T cells but also enhanced their activity, thereby augmenting the antitumor immune response during anti-PD-1 therapy in vivo. This was evidenced by a decrease in CD62L+ CD8T cells and an increase in GZMB+/CD44+/CD69+CD8T cells.

This study has made significant progress in predicting LUAD prognosis and immunotherapy response. Our results indicate that PTMLS is a valuable predictor of immunotherapy response in LUAD, with B4GALT2 emerging as a key gene within PTMLS that can further optimize patient prognostic stratification. Mouse model experiments further confirmed that B4GALT2 may serve as a crucial target influencing immunotherapy efficacy, providing a novel potential target for LUAD immunotherapy strategies. However, we also recognize certain

limitations in our study: first, model validation was limited to B4GALT2 verification using an in-house cohort, lacking broader multicenter clinical validation; second, as a glycosylation-related gene, we primarily investigated B4GALT2’s immune-modulatory role in the tumor microenvironment without delving deeply into its glycosylation-related mechanisms.

Nevertheless, the contributions of this study remain significant. We provide robust evidence supporting B4GALT2 as a potential immunotherapy target, laying the foundation for future research into its immune and glycosylation-related roles in cancer treatment. These findings not only offer new potential targets for LUAD immunotherapy strategies but also indicate directions for subsequent research. Future studies should focus on: expanding the validation scope to include multicenter clinical cohorts to further verify PTMLS’s predictive capability; exploring in-depth the glycosylation-related mechanisms of B4GALT2 to comprehensively understand its role in LUAD development and immune evasion; and developing B4GALT2-based targeted therapeutic strategies while evaluating their synergistic effects with existing immunotherapies. Through these efforts, we aim to provide more precise and effective treatment options for LUAD patients, ultimately improving their prognosis and quality of life.

Author affiliations

¹Department of Lung Cancer, Tianjin Lung Cancer Center, National Clinical Research Center for Cancer, Key Laboratory of Cancer Prevention and Therapy, Tianjin’s Clinical Research Center for Cancer, Tianjin Medical University Cancer Institute and Hospital, Tianjin, China

²Department of Thoracic Surgery, The First Affiliated Hospital of Nanjing Medical University, Nanjing, China

³Department of Cardiology, The First Affiliated Hospital of Zhengzhou University, Zhengzhou, China

Correction notice This article has been corrected since it was first published online. Due to an oversight in the original published article, the incorrect differential gene heatmap was displayed in Figure 2. This has now been corrected.

Acknowledgements We thank The Cancer Genome Atlas (TCGA), Gene Expression Omnibus (GEO), Genome Sequence Archive (GSA), UCSC Xena, Molecular Signature Database (MSigDB), and Tracking Tumor Immunophenotype (TIP) databases for providing the data used in this study.

Contributors The study was conceived and designed by PZ. Data collection was conducted by DW. GZhou and SJ performed the statistical analysis. The first draft of the manuscript was written by PZ and GZhang. The experiment was performed by PZ. The final approval of the submitted version was given by LZ and ZZ. All authors contributed to the manuscript and approved the submitted version. ZZ is responsible for the overall content as the guarantor.

Funding This work was supported by the Tianjin Natural Science Foundation under Grant/Award Number 21JCYBJC01020, and funded by Tianjin Key Medical Discipline (Specialty) Construction Project (TJYXZDXK-011A).

Competing interests None declared.

Patient consent for publication Not applicable.

Ethics approval This study involves human participants and was approved by All human experiments conducted in this study were approved by the Medical Ethics Committee of the Tianjin Medical University Cancer Institute and Hospital (approval number: bc2023152). Participants gave informed consent to participate in the study before taking part.

Provenance and peer review Not commissioned; externally peer reviewed.



Data availability statement Data are available in a public, open access repository. Data are available upon reasonable request.

Supplemental material This content has been supplied by the author(s). It has not been vetted by BMJ Publishing Group Limited (BMJ) and may not have been peer-reviewed. Any opinions or recommendations discussed are solely those of the author(s) and are not endorsed by BMJ. BMJ disclaims all liability and responsibility arising from any reliance placed on the content. Where the content includes any translated material, BMJ does not warrant the accuracy and reliability of the translations (including but not limited to local regulations, clinical guidelines, terminology, drug names and drug dosages), and is not responsible for any error and/or omissions arising from translation and adaptation or otherwise.

Open access This is an open access article distributed in accordance with the Creative Commons Attribution Non Commercial (CC BY-NC 4.0) license, which permits others to distribute, remix, adapt, build upon this work non-commercially, and license their derivative works on different terms, provided the original work is properly cited, appropriate credit is given, any changes made indicated, and the use is non-commercial. See <http://creativecommons.org/licenses/by-nc/4.0/>.

Author note AI technology used: ChatGPT (OpenAI). Purpose of use: For language editing and polishing to improve the manuscript's linguistic quality and readability. Method of use: We used ChatGPT for grammar checking, technical terminology verification, and sentence structure enhancement in the Introduction, Results, and Discussion sections. All AI-assisted content was thoroughly reviewed by Pengpeng Zhang to ensure scientific accuracy, proper use of technical terminology, and consistency with our original research findings.

ORCID iD

Pengpeng Zhang <http://orcid.org/0000-0002-9627-2590>

REFERENCES

- 1 Wang M, Herbst RS, Boshoff C. Toward personalized treatment approaches for non-small-cell lung cancer. *Nat Med* 2021;27:1345–56.
- 2 Liang G, Meng W, Huang X, et al. miR-196b-5p-mediated downregulation of TSPAN12 and GATA6 promotes tumor progression in non-small cell lung cancer. *Proc Natl Acad Sci U S A* 2020;117:4347–57.
- 3 Alexander M, Kim SY, Cheng H. Update 2020: Management of Non-Small Cell Lung Cancer. *Lung* 2020;198:897–907.
- 4 Wang S, Wang R, Hu D, et al. Machine learning reveals diverse cell death patterns in lung adenocarcinoma prognosis and therapy. *NPJ Precis Oncol* 2024;8:49.
- 5 Yang T, Xiong Y, Zeng Y, et al. Current status of immunotherapy for non-small cell lung cancer. *Front Pharmacol* 2022;13:989461.
- 6 Lahiri A, Maji A, Potdar PD, et al. Lung cancer immunotherapy: progress, pitfalls, and promises. *Mol Cancer* 2023;22:40.
- 7 Li Y, Zhang R, Hei H. Advances in post-translational modifications of proteins and cancer immunotherapy. *Front Immunol* 2023;14:1229397.
- 8 Czuba LC, Hillgren KM, Swaan PW. Post-translational modifications of transporters. *Pharmacol Ther* 2018;192:88–99.
- 9 Fang Y, Xu X, Ding J, et al. Histone crotonylation promotes mesoendodermal commitment of human embryonic stem cells. *Cell Stem Cell* 2021;28:748–63.
- 10 Kukkula A, Ojala VK, Mendez LM, et al. Therapeutic Potential of Targeting the SUMO Pathway in Cancer. *Cancers (Basel)* 2021;13:4402.
- 11 Liu X, Zhang Y, Wang Y, et al. Protein Phosphorylation in Cancer: Role of Nitric Oxide Signaling Pathway. *Biomolecules* 2021;11:1009.
- 12 Cruz Walma DA, Chen Z, Bullock AN, et al. Ubiquitin ligases: guardians of mammalian development. *Nat Rev Mol Cell Biol* 2022;23:350–67.
- 13 Dang F, Nie L, Wei W. Ubiquitin signaling in cell cycle control and tumorigenesis. *Cell Death Differ* 2021;28:427–38.
- 14 Dai X, Lu L, Deng S, et al. USP7 targeting modulates anti-tumor immune response by reprogramming Tumor-associated Macrophages in Lung Cancer. *Theranostics* 2020;10:9332–47.
- 15 Cheng J, Yan J, Liu Y, et al. Cancer-cell-derived fumarate suppresses the anti-tumor capacity of CD8⁺ T cells in the tumor microenvironment. *Cell Metab* 2023;35:961–78.
- 16 Yang H, Zou X, Yang S, et al. Identification of lactylation related model to predict prognostic, tumor infiltrating immunocytes and response of immunotherapy in gastric cancer. *Front Immunol* 2023;14:1149989.
- 17 Magalhães A, Duarte HO, Reis CA. The role of O-glycosylation in human disease. *Mol Aspects Med* 2021;79:100964.
- 18 Hu X, Lin Z, Wang Z, et al. Emerging role of PD-L1 modification in cancer immunotherapy. *Am J Cancer Res* 2021;11:3832–40.
- 19 Gulhane P, Singh S. Unraveling the Post-Translational Modifications and therapeutic approach in NSCLC pathogenesis. *Transl Oncol* 2023;33:101673.
- 20 Tomida S, Takeuchi T, Shimada Y, et al. Relapse-related molecular signature in lung adenocarcinomas identifies patients with dismal prognosis. *J Clin Oncol* 2009;27:2793–9.
- 21 Wilkerson MD, Yin X, Walter V, et al. Differential pathogenesis of lung adenocarcinoma subtypes involving sequence mutations, copy number, chromosomal instability, and methylation. *PLoS ONE* 2012;7:e36530.
- 22 Staaf J, Jönsson G, Jönsson M, et al. Relation between smoking history and gene expression profiles in lung adenocarcinomas. *BMC Med Genomics* 2012;5:22.
- 23 Rousseaux S, Debernardi A, Jacquiau B, et al. Ectopic activation of germline and placental genes identifies aggressive metastasis-prone lung cancers. *Sci Transl Med* 2013;5:186ra66.
- 24 Okayama H, Kohno T, Ishii Y, et al. Identification of genes upregulated in ALK-positive and EGFR/KRAS/ALK-negative lung adenocarcinomas. *Cancer Res* 2012;72:100–11.
- 25 Tang H, Xiao G, Behrens C, et al. A 12-gene set predicts survival benefits from adjuvant chemotherapy in non-small cell lung cancer patients. *Clin Cancer Res* 2013;19:1577–86.
- 26 Rittmeyer A, Barlesi F, Waterkamp D, et al. Atezolizumab versus docetaxel in patients with previously treated non-small-cell lung cancer (OAK): a phase 3, open-label, multicentre randomised controlled trial. *Lancet* 2017;389:255–65.
- 27 Fehrenbacher L, Spira A, Ballinger M, et al. Atezolizumab versus docetaxel for patients with previously treated non-small-cell lung cancer (POPLAR): a multicentre, open-label, phase 2 randomised controlled trial. *Lancet* 2016;387:1837–46.
- 28 Ravi A, Hellmann MD, Arniella MB, et al. Genomic and transcriptomic analysis of checkpoint blockade response in advanced non-small cell lung cancer. *Nat Genet* 2023;55:807–19.
- 29 Cho J-W, Hong MH, Ha S-J, et al. Genome-wide identification of differentially methylated promoters and enhancers associated with response to anti-PD-1 therapy in non-small cell lung cancer. *Exp Mol Med* 2020;52:1550–63.
- 30 Lee JS, Nair NU, Dinstag G, et al. Synthetic lethality-mediated precision oncology via the tumor transcriptome. *Cell* 2021;184:2487–502.
- 31 Hu J, Zhang L, Xia H, et al. Tumor microenvironment remodeling after neoadjuvant immunotherapy in non-small cell lung cancer revealed by single-cell RNA sequencing. *Genome Med* 2023;15:14.
- 32 Jung H, Kim HS, Kim JY, et al. DNA methylation loss promotes immune evasion of tumours with high mutation and copy number load. *Nat Commun* 2019;10:4278.
- 33 Riaz N, Havel JJ, Makarov V, et al. Tumor and Microenvironment Evolution during Immunotherapy with Nivolumab. *Cell* 2017;171:934–49.
- 34 Van Allen EM, Miao D, Schilling B, et al. Genomic correlates of response to CTLA-4 blockade in metastatic melanoma. *Science* 2015;350:207–11.
- 35 Lauss M, Donia M, Harbst K, et al. Mutational and putative neoantigen load predict clinical benefit of adoptive T cell therapy in melanoma. *Nat Commun* 2017;8:1738.
- 36 Zhao J, Chen AX, Gartrell RD, et al. Immune and genomic correlates of response to anti-PD-1 immunotherapy in glioblastoma. *Nat Med* 2019;25:462–9.
- 37 Braun DA, Hou Y, Bakouny Z, et al. Interplay of somatic alterations and immune infiltration modulates response to PD-1 blockade in advanced clear cell renal cell carcinoma. *Nat Med* 2020;26:909–18.
- 38 Zhang Y, Parmigiani G, Johnson WE. ComBat-seq: batch effect adjustment for RNA-seq count data. *NAR Genom Bioinform* 2020;2:lqaa078.
- 39 Zhang L, Cui Y, Zhou G, et al. Leveraging mitochondrial-programmed cell death dynamics to enhance prognostic accuracy and immunotherapy efficacy in lung adenocarcinoma. *J Immunother Cancer* 2024;12:e010008.
- 40 Wu T, Hu E, Xu S, et al. clusterProfiler 4.0: A universal enrichment tool for interpreting omics data. *Innov Camb* 2021;2:100141.
- 41 Xu L, Deng C, Pang B, et al. TIP: A Web Server for Resolving Tumor Immunophenotype Profiling. *Cancer Res* 2018;78:6575–80.
- 42 Hu J, Yu A, Othmane B, et al. Siglec15 shapes a non-inflamed tumor microenvironment and predicts the molecular subtype in bladder cancer. *Theranostics* 2021;11:3089–108.



- 43 Zeng D, Ye Z, Shen R, et al. IOBR: Multi-Omics Immuno-Oncology Biological Research to Decode Tumor Microenvironment and Signatures. *Front Immunol* 2021;12:687975.
- 44 Cao Y, Fu L, Wu J, et al. Integrated analysis of multimodal single-cell data with structural similarity. *Nucleic Acids Res* 2022;50:e121.
- 45 Wang Z, Li Z, Zhou K, et al. Deciphering cell lineage specification of human lung adenocarcinoma with single-cell RNA sequencing. *Nat Commun* 2021;12:6500.
- 46 Jin S, Guerrero-Juarez CF, Zhang L, et al. Inference and analysis of cell-cell communication using CellChat. *Nat Commun* 2021;12:1088.
- 47 Wang Y, Deng J, Wang L, et al. Expression and clinical significance of PD-L1, B7-H3, B7-H4 and VISTA in craniopharyngioma. *J Immunother Cancer* 2020;8:e000406.
- 48 Liu A, Yu C, Qiu C, et al. PRMT5 methylating SMAD4 activates TGF- β signaling and promotes colorectal cancer metastasis. *Oncogene* 2023;42:1572–84.
- 49 Yang Z, Yan C, Ma J, et al. Lactylome analysis suggests lactylation-dependent mechanisms of metabolic adaptation in hepatocellular carcinoma. *Nat Metab* 2023;5:61–79.
- 50 Gao G-B, Sun Y, Fang R-D, et al. Post-translational modifications of CDK5 and their biological roles in cancer. *Mol Biomed* 2021;2:22.
- 51 Wang X, Zhang Y, Wu Y, et al. The role of E3 ubiquitin ligases and deubiquitinases in bladder cancer development and immunotherapy. *Front Immunol* 2023;14:1202633.
- 52 Zhao R, Qin W, Qin R, et al. Lectin array and glycogene expression analyses of ovarian cancer cell line A2780 and its cisplatin-resistant derivate cell line A2780-cp. *Clin Proteomics* 2017;14:20.
- 53 Venkitachalam S, Revoredo L, Varadan V, et al. Biochemical and functional characterization of glycosylation-associated mutational landscapes in colon cancer. *Sci Rep* 2016;6:23642.